Magneto-optical properties of Rare Earth metals substituted Co-Zn spinel nanoferrites

M.A. Almessiere[a,b] A.D. Korkmaz[c1,], Y. Slimani[d], M. Nawaz[b], S. Ali[e], A. Baykal[b]

[a]Department of Physics, College of Science; [b]Department of Nano-Medicine Research, [d]Department of Biophysics, Institute for Research & Medical Consultations (IRMC);

[e]Department of Mechanical and Energy Engineering, College of Engineering, Imam Abdulrahman Bin Faisal University, 31982, Dammam, Saudi Arabia

[c]Department of Chemistry, Istanbul Medeniyet University, 34700 Uskudar, Istanbul/Turkey

Abstract

Cobalt–zinc ferrite nanoparticles (NPs) substituted with three different metals, $Co_{0.5}Zn_{0.5}Re_xFe_{2-x}O_4$ (RE = Ce, Dy, and Y; $0.00 \leqslant x \leqslant 0.05$) were prepared hydrothermally. Fourier Transform-Infrared (FT-IR) Spectroscopy, X-ray powder diffraction (XRD), Field-Emission Scanning Electron Microscope (FESEM) coupled with energy-dispersive X-ray spectroscopy (EDX) and Vibrating Sample Magnetometry (VSM) analyzed the products. The formation of cubic phase of spinel Co-Zn ferrite NPs were confirmed through XRD, FT-IR and FE-SEM techniques. The structural investigation of NPs by XRD revealed that the lattice parameter "a" decreases with the

[1]Corresponding author's E-mail: ayse.demir@medeniyet.edu.tr (Ayse Demir Korkmaz). Phone: +90-216-280-3449

introduction of the RE in the ferrite structure by the substitution of Fe^{3+} by RE ions. The different magnetic parameters of $Co_{0.5}Zn_{0.5}Re_xFe_{2-x}O_4$ (RE = Ce, Dy, and Y; $0.00 \leqslant x \leqslant 0.05$) NPs such as the saturation magnetization, coercivity, remanence, and magnetic moment were calculated and discussed in relation to structure and microstructure properties. M (H) hysteresis curves indicated that the samples exhibit superparamagnetic nature at room temperature. A slight improvement in the magnetization was obtained especially for the Ce- and Y-substituted $Co_{0.5}Zn_{0.5}Fe_2O_4$ (CZF) NPs at a certain RE level. However, the case Dy-substituted CZF products showed a sharp decrease in the magnetization with $x > 0.01$. The results are mostly ascribed to the substitution of smaller Fe^{3+} ions with larger RE^{3+} ions.

Keywords: Spinel ferrites; Rare earth substitution; Hydrothermal; Morphology; Magnetic properties.

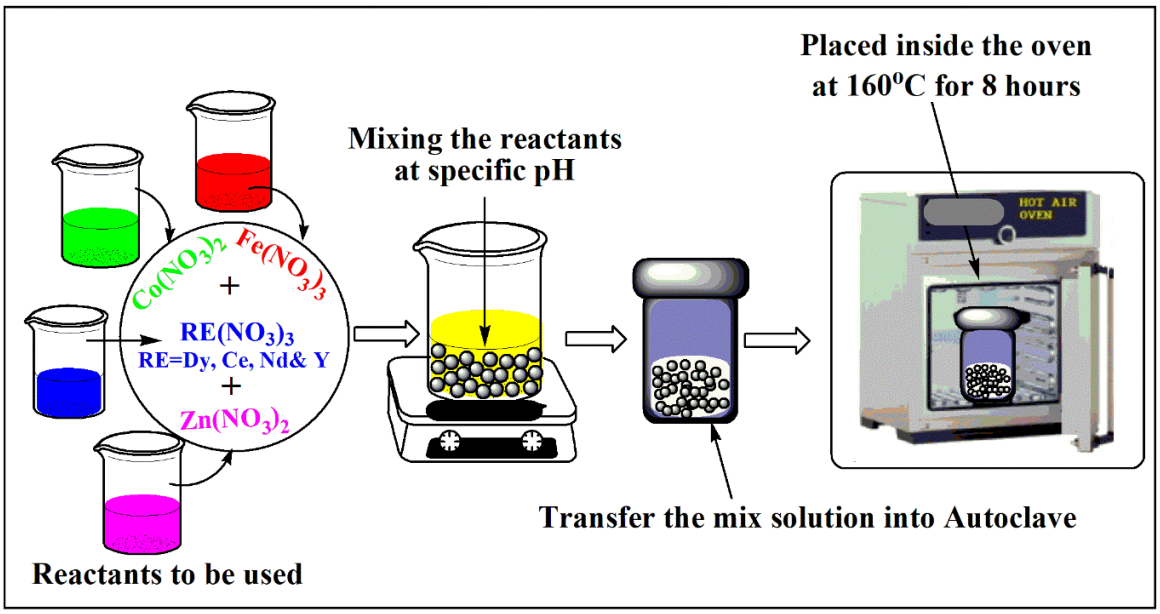

Graphical Abstract for the synthesis of Nanoparticles

1. Introduction

Ferrites are the combination of iron oxides and metals, which have been mostly used in electromagnetic and biotechnology applications [1,2]. Ferrites have extraordinary, electrical-chemical stability, mechanical hardness and high permeability properties that are mostly preferred in high-frequency devices [3]. Spinel ferrite (MFe_2O_4) is a face center cubic (FCC) structure, whereas oxygen represents anions and 'M' metal cations e.g., Mg^{2+}, Cd^{2+}, Mn^{2+}, Co^{2+}, Zn^{2+}, Ni^{2+}. A spinel ferrite unit cell contains eight formula units whereas each unit cell comprises of 64 and 32 tetrahedral (A) sites and octahedral (B) sites, respectively [4]. Spinel ferrites are very ideal and suitable materials in various technological and industrial application like high-density storage media, electrochemical supercapacitive material, microwave absorbers, transformer cores, rod antennas, gas sensing elements, hypothermia for cancer treatment and magnetic drug delivery [5–8]. Many researchers have been investigated that physical, dielectric, magnetic, optical and chemical characteristics are depends upon the composition, substitution, and methods of preparation [6,9]. The effect of electromagnetic properties depends by substituting the metal ions into spinel structure [10].

The rare earth ions with a stable valence of 3+ and large radius that can be made appropriate modification the ferrites structure. Furthermore, the rare earth is an alternative and economical source to improve electromagnetic properties [11]. Numbers of devices have been focused to improve the superparamagnetic and ferrimagnetic properties, besides that quantum tunneling effect has been achieved by nano-magnetism in ferrimagnetic materials [12]. The rare earth doping in nanospinel ferrites is highly recommended to enhance the electric and magnetic

properties of the ferrites (due to their strong spin-orbit coupling of unpaired 4f electrons) [13-16]. Lanthanides series (Ce to Y) are the specific concern as the dopant in ferrites [17]. Rare earth substitution in ferrites can be easily induced the increasing ionic radii, micro-strain and control the magnetic parameters [18]. The electromagnetic properties subjected by spin coupling of the 3*d* electrons. The magnetic and electrical properties improved when rare earth ions incorporate the spinel lattice and great interaction of rare earth and iron (3*d*–4*f* coupling) of the ferrites [19]. It has been reported that the rare earth substitution is very useful to intensification the lattice parameter and reduced the particle size of the NPs [20]. Similarly, the incorporation of Gd^{3+} ions in cobalt zinc ferrite has been improved the electrical and elastic properties of ferrites [21]. The substitution of Sm^{3+} and Pr^{3+} ions displays the high magnetization of spinel ferrite [22]. The doping of rare earth ions in Ni-Zn ferrites reduced the dielectric loss that is highly recommended for high-frequency applications [23]. It has been published that magnetic loss and permeability can be increase by La^{3+} substitution in Ni-Cu-Zn ferrite [24]. The doping of Dy^{3+} and Ce^{3+} ions in Co-Zn ferrite are very suitable for increase the magnetic hardness and magneto-caloric applications [19,25].

In this paper, the influence of the incorporation of RE (Ce, Dy and Y) on the morphological, structural, and magnetic properties of $Co_{0.5}Zn_{0.5}Fe_2O_4$ NPs synthesized by hydrothermal method were explored.

2. Experimental

2.1. Materials and Instrumentation

$Co_{0.5}Zn_{0.5}Re_xFe_{2-x}O_4$ (RE = Ce, Dy, and Y; 0.00 ⩽ x ⩽ 0.05) NPs were synthesized hydrothermally. Zinc (II) nitrate ($Zn(NO_3)_2$), Iron (III) nitrate hexahydrate ($Fe(NO_3)_3{\cdot}6H_2O$), Cobalt (II) nitrate ($Co(NO_3)_2$), Cerium (III) nitrate ($Ce(NO_3)_2$), Dysprosium (III) nitrate ($Dy(NO_3)_3$) and Yttrium Nitrate ($Y(NO_3)_3{\cdot}6H_2O$) were employed as initial materials for preparation. All chemicals were purchased from Merck and used without further purification. The XRD analysis was conducted by a Rigaku Benchtop Miniflex X-ray diffractometer with Cu K_α radiation at room temperature (RT). Fourier transform-infrared spectra were recorded using a Bruker FT-IR spectrometer between wavenumbers 4000–400 cm^{-1}. A field-emission scanning electron microscope (FESEM; FEI Titan S/T) coupled with energy-dispersive X-ray spectroscopy (EDX) was used to investigate the ferrite particle morphology. Magnetic properties of the ferrites were analyzed using a Quantum Design SQUID with a vibrating sample magnetometer (VSM) head at RT. Optical properties of NPs were studied by a Visible Evolution 220 Thermo UV Spectrophotometer with an Integrating Sphere Accessory for diffuse reflectance (DR) studies.

2.2. Method

$Co_{0.5}Zn_{0.5}Re_xFe_{2-x}O_4$ (RE = Ce, Dy, and Y; 0.00 ⩽ x ⩽ 0.05) NPs were fabricated hydrothermally. For each composition, stoichiometric amounts of Co (II), Zn (II), and Fe (III) nitrate salts were dissolved in 15 ml of H_2O then diluted to 30 ml with DI H_2O. In addition, the stoichiometric amount of $Ce(NO_3)_3$ salt was dissolved in 7 ml of concentrated HCl by heating and stirring. Then two metal nitrate solutions were added to a flask, stirred for 30 min. Next, NaOH solution was added to the metal precursor mixture to adjust the pH to 12, which was

followed by continuous stirring for another 30 min. The mixture then was pre-treated in an ultrasonic bath during 30–40 min. The final solution was transferred to a stainless steel Teflon autoclave (200 ml) and kept in an oven at 180°C for 10h. The powder obtained was washed with three times with DI H_2O and left to dry overnight. Subsequently, the solid product was calcined in a muffle furnace at 800°C for 5 h. Dy and Y substituted $Co_{0.5}Zn_{0.5}RE_xFe_{2-x}O_4$ ($0.0 \leq x \leq 0.5$) NPs were prepared with the same procedure above [26].

3. Results and discussion

3.1. XRD analysis

The X-ray powder patterns of $Co_{0.5}Zn_{0.5}Re_xFe_{2-x}O_4$ (RE = Ce, Dy, and Y; $0.00 \leqslant x \leqslant 0.05$) NPs are displayed in Fig. 1, which confirmed spinel structure formation with the (220), (311), (400), (422), (511) and (440) hkl values (JCPDS Card No: 96-153-5821). No peaks belong to additional second phase were detected. Furthermore, it was approved that the RE are distributed well throughout the cobalt spinel crystal. The structural parameters are calculated through Rietveld refinements by Match 3! Software and presented in Table 1. It is expected that the lattice parameter 'a' will increase because of the substitutions of RE atoms which a larger size with the host Fe atoms which have a smaller size. However, it is noticeable in this study that the lattice parameter "a" is decreased with introducing the RE in the ferrite structure. Indeed, the introduction of larger RE^{3+} ions into the structure of CZF will lead to distort the octahedral and tetrahedral symmetry. This results in to create of Fe vacancies that could decrease the lattice parameter [27]. The average crystallites sizes (D_{XRD}) were calculated for all compositions and

are presented in Fig. 2. The obtained values of D_{XRD} ranging between 7.5 and 11.7 nm for different produced $Co_{0.5}Zn_{0.5}Re_xFe_{2-x}O_4$ (RE = Ce, Dy, and Y; $0.00 \leqslant x \leqslant 0.05$) NPs.

Table 1.

Fig. 1.

Fig. 2.

3.2. FT-IR analysis

FT-IR spectra of $Co_{0.5}Zn_{0.5}Re_xFe_{2-x}O_4$ (RE = Ce, Dy, and Y; $0.00 \leqslant x \leqslant 0.05$) NPs are displayed in Fig. 3. All compositions demonstrate the characteristic peaks of cobalt ferrite around 571 and 400 cm^{-1}. These peaks correspond to Co-O and Fe-O bonds [28]. It was found that the peak at 571 cm^{-1} shifted toward higher frequency since the distance between Fe^{3+}– O^{2-} decreases [29]. The bands at 2979 and 1056 cm^{-1} can be assigned to C-H and C-C bands, which result from the combustion of citric acid during the preparation process, while the band at 1360 cm^{-1} is assigned to NO_3^- group.

Fig. 3.

3.3. % Diffuse Reflectance study

Optical properties of $Co_{0.5}Zn_{0.5}Re_xFe_{2-x}O_4$ (RE = Ce, Dy, and Y; $0.00 \leqslant x \leqslant 0.05$) NPs were studied by a UV-Vis spectrophotometer with an integrating sphere attachment for the measurement of diffuse reflectance. The % DR spectra of $Co_{0.5}Zn_{0.5}Re_xFe_{2-x}O_4$ (RE = Ce, Dy, and Y; $0.00 \leqslant x \leqslant 0.05$) NPs at different composition were recorded in the 200-800 nm wavelength range and are depicted in Fig. 4-6. It can also be inferred from both figures that all spectra absorb the light energy. The band gap energy (E_g) of all products was studied by Kubelka-Munk theory [30]. The band gap energy of the NPs was computed by the Tauc equation as stated in [30] and displayed as the plots $(\alpha hv)^2$ *vs.* photon energy (hv) (Fig. 4-6).

The band gap values for $Co_{0.5}Zn_{0.5}Ce_xFe_{2-x}O_4$ ($0.00 \leqslant x \leqslant 0.05$) NPs are shown in Fig. 4 and are 0.77, 0.26, 0.25 and 0.25 eV for x= 0.00, 0.01, 0.03 and 0.05, respectively. It can be easily concluded that when value of x is increased, the band gap value is reduced. However, no significant variation was observed for different concentrations. Fig. 5 shows the plot of $(\alpha hv)^2$ *vs.* (hv) for $Co_{0.5}Zn_{0.5}Dy_xFe_{2-x}O_4$ ($0.00 \leqslant x \leqslant 0.05$) NPs. The band gap values obtained were 0.49, 0.24 and 0.18 eV for x = 0.01, 0.03 and 0.05, respectively. The band gap value for $Co_{0.5}Zn_{0.5}Dy_xFe_{2-x}O_4$ NPs became quite narrow upon increasing concentration of x.

The band gap values for $Co_{0.5}Zn_{0.5}Y_xFe_{2-x}O_4$ ($0.00 \leqslant x \leqslant 0.05$) NPs were observed 0.24, 0.22 and 0.23 eV for x= 0.01, 0.03 and 0.05 respectively as shown in Fig. 6. It was noticed that the increase in concentration does not display a substantial change on the band gap of $Co_{0.5}Zn_{0.5}Y_xFe_{2-x}O$. However, as compared to x= 0.00, the band gap value of $Co_{0.5}Zn_{0.5}Y_xFe_{2-x}O_4$ was reduced in other samples.

Fig. 4.

Fig. 5.

Fig. 6.

3.4. Morphological analysis

Further structural evaluation of $Co_{0.5}Zn_{0.5}Re_xFe_{2-x}O_4$ (RE = Ce, Dy, and Y; $0.00 \leqslant x \leqslant 0.05$) NPs was accomplished by SEM and EDX (Fig. 7 and Fig. 8). The images exhibited highly agglomerated nanoparticles with inhomogeneous distribution, which is similar in all compositions. This is most probably due to the magnetic dipole interactions between these nanoparticles. The EDX analysis approved the presence of RE in the prepared samples as shown in Fig. 8. For all products, the experimental values are in well agreement with the calculated values indicating that RE substituted $Co_{0.5}Zn_{0.5}$ spinel ferrites were successfully synthesized.

Fig. 7.

Fig. 8.

3.5. VSM Analysis

The PPMS-VSM method was employed to explore the magnetic behavior of spinel ferrite NPs under a magnetic field, M (H) between -10 kOe and 10 kOe at RT. Figure 9 shows the M (H) hysteresis loops of $Co_{0.5}Zn_{0.5}Re_xFe_{2-x}O_4$ (RE = Ce, Dy, and Y; $0.00 \leqslant x \leqslant 0.05$) NPs where the saturation magnetization (M_s), retentivity (M_r) and coercive field (H_c) can be deduced. The magnetic field applied is enough for saturating the various produced NPs. Stoner-Wohlfarth (SW) approximation was used to calculate M_s values [31, 32]. A typical example for determining value of M_s for x=0.0 sample by the extrapolation of the curves of M vs. $1/H^2$ plot to approach zero is illustrated as seen in Figure 10. Synthesized ferrites exhibit values of M_s varying in the ranges of 34.7 – 40.8 emu·g^{-1}, 13.6 – 39.9 emu·g^{-1} and 35.2 – 41.8 emu·g^{-1} for $Co_{0.5}Zn_{0.5}Ce_xFe_{2-x}O_4$, $Co_{0.5}Zn_{0.5}Dy_xFe_{2-x}O_4$ and $Co_{0.5}Zn_{0.5}Y_xFe_{2-x}O_4$ NPs respectively. The values of remanent magnetization (M_r) are in the intervals of 0.23 – 2.20 emu·g^{-1}, 0.16 – 2.03 emu/g and 1.64 – 2.51 emu·g^{-1} for Ce-, Dy- and Y-substituted CZF products, respectively. The coercivity (H_c) is very narrow for various ferrite products. Therefore, it can be deduced that the $Co_{0.5}Zn_{0.5}RE_xFe_{2-x}O_4$ (RE = Ce, Dy and Y; $0.00 \leq x \leq 0.05$) NPs display a superparamagnetic (SPM) behavior.

The various determined magnetic parameters of M_s, M_r, H_c and SQR (squareness ratio), which is defined as the ratio of M_r/M_s, for different $Co_{0.5}Zn_{0.5}RE_xFe_{2-x}O_4$ (RE = Ce, Dy and Y; $0.00 \leq x \leq 0.05$) nanoparticles are recorded in Table 2. The value of M_s of the pristine sample (x = 0.0) is about 39.9 emu·g^{-1}. The M_s value found in the present work for CZF NPs is smaller than the M_s of bulk CZF ferrite (~80 emu·g^{-1}) [33, 34]. In addition, the obtained values of M_s found in our study for various products are greater than that of CZF NPs studied in previous reports [35, 36]. The lower M_s value in comparison to bulk product is mainly a result of small size of crystallites that conduces to a structural disorder on the surfaces of NPs because the spins disorder is important once the ratio between surface

and volume is important [37]. Other factors that might play a role in the low M_s values in NPs can be the formation of a magnetic dead layer, disorderly cation distribution on NP surfaces, the spin canting effect due to competing antiferromagnetic interactions, etc. [38, 39]. Any variation in the nature and concentration of ions in A and B sites results in different values of magnetization when compared to the reference values. The values of M_s do not exhibit a similar trend in different synthesized products for the same level of RE concentration (x). For $Co_{0.5}Zn_{0.5}Ce_xFe_{2-x}O_4$ ($0.00 \leq x \leq 0.05$) NPs, the value of M_s increases slightly for x = 0.01 compared to the sample where x = 0.00 and then decreases with further increasing Ce content. In the case of Dy-substituted CZF NPs, the M_s shows a sharp decrease with x > 0.01. For Y-substituted CZF NPs, M_s values are comparable for x = 0.00 and 0.01 products, decrease when x = 0.03 and then increase when x = 0.05 with the M_s being greater than that of pristine sample. Generally, the magnetic properties of spinel ferrites are greatly affected by various factors such as the variation in the crystallites size, changes in the magnetic moments (n_B), preferred site occupancy of different ions, and formation of local strains. [40-43]. The disordered cation distributions and the super-exchange interactions among various ions may also play a role on the magnetic properties [40]. As it is widely known, the magnetic moment of spinel ferrites originates from the Fe^{3+} ions. The magnetization of the ferrites is mainly ruled by the distribution of iron ions in the crystal lattice sites and thus varies with the elements which affect the strength of the exchange interactions in the Fe^{3+}-O-Fe^{3+} linkage (spin couplings of the 3d electrons) [40, 44]. After the inclusion of RE ions inside the crystallographic lattice, the RE^{3+}-O-Fe^{3+} exchange interactions take place through the 4f–3d couplings and start to have a considerable influence. The RE-O-Fe interactions could result in changing in the magnetizations. Nevertheless, because they are derived from the indirect 4f–5d–5d–4f couplings, the interactions between RE-O-RE are considerably weak [40, 44]. A-B exchange interactions can be accounted

responsible for the improvement (or decrease) in the M_s value with RE-substitutions. In the ferrites, trivalent ions strongly prefer to occupy B sites, whereas divalent ones may occupy both A and B sites. In addition, the site preference of different ions is dependent on the radii of host and substituted ions. The ionic radii of Fe^{3+} ions are smaller than of the radii of ions of RE elements. It is well known that the B sites are greater when compared with A sites and it can be anticipated that the A site will be preferred by the smaller ions [44]. Therefore, the replacement of Fe^{3+} (0.64 Å) by RE^{3+} (> 0.9 Å in this study) on the B sites, which is principally responsible for magnetization can explain the reduction in magnetization. In addition, the ions of Fe^{3+} substituted by RE ions that exhibit greater ionic radius will lead to increase the distances among different ions, and as consequence the A-B exchange interactions strength will be reduced. In addition, the spins will be the dominant and powerful factor owing to the quenching of the orbital momentum [44]. This will result in a reduction in the magnetization. The RE^{3+} ions are greatly paramagnetic (PM) in nature; therefore, the ferromagnetic (FM) region is reduced while the PM increases by the replacement of Fe^{3+} ions by RE ions [44]. In addition, the larger radius of RE^{3+} ions compared to Fe^{3+} ions will result in an incomplete introduction of all the RE ions into the crystallographic lattice of the ferrites. Consequently, some RE^{3+} ions possibly reside at grains boundaries and create ultra-thin isolating layers around the grains during the sintering stage [45]. This could decrease the strength of magnetic interactions and lead to a decrease in the M_s. Moreover, the difference in the ionic radius and magnetic moments of the host and substituted ions could generate local strains that cause the deviations in the electronic states and the disorder in the ferrite system [40-43]. Furthermore, the variation in the values of the n_B could explain the behavior of M_s. The experimental values of n_B are deduced via the following expression [42]:

$$n_B = (Molecular\ weight\ x\ M_s)/5585$$

The calculated values of n_B for $Co_{0.5}Zn_{0.5}RE_xFe_{2-x}O_4$ (RE = Ce, Dy and Y; $0.00 \leq x \leq 0.05$) NPs are listed in Table 2. It is well known that the n_B values are increased (or reduced) due to a rise (or decline) in the super exchange interactions among the A and B sites. It was found in the present study that the product with the highest M_s value exhibits the highest n_B value. This is a consequence of the intensification of super exchange interactions among the A and B sites. In contrast, the lowest n_B value is expressed by the product with lowest M_s value. As mentioned above, the variations in the average grain size or average particle size have an influence on the magnetic characteristics of spinel ferrites. Usually, the values of magnetic parameters decrease with decreasing the average grains size. Vice versa, the values of magnetic parameters increase with increasing the average grains size. In the present work, the variations of average crystallites size as shown in Fig. 2 exhibit a similar trend of M_s evolutions.

The changes in M_r with respect to the content of RE substitutions show practically the similar evolution tendencies of the M_s. It was noted that the evolution in the M_r values is dependent primarily on the change in saturation magnetization values and on the net alignment of the magnetization of grains induced from the super exchange interactions among NPs [46-48]. For $Co_{0.5}Zn_{0.5}Ce_xFe_{2-x}O_4$, $Co_{0.5}Zn_{0.5}Dy_xFe_{2-x}O_4$ and $Co_{0.5}Zn_{0.5}Y_xFe_{2-x}O_4$ NPs, SQR values are found to be in the ranges of 0.007 – 0.054, 0.028 – 0.051 and 0.047 – 0.060, respectively. Consistent with S-W law, the SQR was calculated as 0.830 and 0.500 for cubic and uniaxial anisotropy, respectively [31, 49]. The obtained values of SQR are below the 0.500 value, revealing the uniaxial anisotropy for various synthesized $Co_{0.5}Zn_{0.5}RE_xFe_{2-x}O_4$ (RE = Ce, Dy and Y; $0.00 \leq x \leq 0.05$) NPs. In addition, the SQR values are much lower than 0.5, which may possibly be ascribed to the effects of surface spin disorder. The values of H_c are found to be in the intervals of 43.1 – 57.3 Oe, 25.2 – 50.5 Oe and 31.9 – 61.2 Oe for Ce-, Dy- and Y-substituted CZF NPs, respectively. Nevertheless, the values of H_c and M_r are

negligible, indicating the SPM behavior in various produced NPs. In general, the coercivity depends on several factors including the magneto-crystalline anisotropy, morphology, size distribution, grain size, shape anisotropy, exchange coupling between the collinear spins in the core and the canted spins on the surface, etc. [50-52]. It is known that the variation of H_c and crystallites size possess reciprocal relation. In this study, it can be clearly observed that the increase (or decrease) in D_{XRD} is followed by a decrease (or increase) in H_c.

Fig. 9.

Fig. 10.

Table 2.

4. Conclusion

$Co_{0.5}Zn_{0.5}RE_xFe_{2-x}O_4$ (RE = Ce, Dy, and Y; $0.00 \leqslant x \leqslant 0.05$) NPs were successfully prepared through hydrothermal process. The formation of cubic phase of spinel Co-Zn ferrite NPs was confirmed by FT-IR, XRD, FE-SEM and EDX. The lattice parameter "a" is decreased with the introduction of the RE in the ferrite structure. It was found that the introduction of larger RE^{3+} ions into the structure of CZF NPs leads to a distortion in the octahedral and tetrahedral symmetry and hence tend to build Fe vacancies, which decreases the lattice parameter. The magnetic properties of $Co_{0.5}Zn_{0.5}RE_xFe_{2-x}O_4$ (RE = Ce, Dy, and Y; $0.00 \leqslant x \leqslant 0.05$) NPs were analyzed by VSM. The M (H) hysteresis loops indicated superparamagnetic nature at room temperature for different synthesized products. The magnetizations are slightly improved at a certain RE level for the Ce- and Y-substituted CZF NPs. However, the magnetization values displayed a sharp decrease for the Dy-substituted CZF NPs with $x > 0.01$. The substitution of Fe^{3+} ions of smaller ionic radii with RE^{3+} ions of larger ionic radii can be held accountable for the results obtained. The improvement (or decrease) in the values of various magnetic parameters with RE-substitutions is attributed to the site preference of different ions. That depends on the ionic radii of host and substituted ions, to the strengthening (or reduction) of the A-B exchange interactions, the generation of local strains, the increase (or decrease) in values of magnetic moment n_B, and the increase (or decrease) of average crystallites sites.

Acknowledgments

Authors are grateful to the Institute for Research & Medical Consultations (IRMC) of Imam Abdulrahman Bin Faysal University for the financial assistance to pursue this research (Grant

No: 2018-IRMC-S-1). The technical assistance provided by Core Labs of King Abdullah University of Science and Technology (KAUST) are highly appreciated.

References

[1] R.H. Kadam, K. Desai, V.S. Shinde, M. Hashim, S.E. Shirsath, Influence of Gd^{3+} ion substitution on the $MnCrFeO_4$ for their nanoparticle shape formation and magnetic properties, J. Alloys Compd. 657 (2016) 487–494.

[2] S. Karimunnesa, A.K.M.A. Ullah, M.R. Hasan, F.S. Shanta, R. Islam, M.N.I. Khan, Effect of holmium substitution on the structural, magnetic and transport properties of CoFe2-xHoxO4 ferrites, J. Magn. Magn. Mater. 457 (2018) 57–63.

[3] A. P. Subramanian, S. K. Jaganathan, A. Manikandan, K. N. Pandiaraj, Gomathi N, E. Supriyanto, Recent trends in nano-based drug delivery systems for efficient delivery of phytochemicals in chemotherapy, RSC Advances 6 (2016) 48294-48314.

[4] A. G. Abraham, A. Manikandan, E. Manikandan, S. Vadivel, S.K. Jaganathan, A. Baykal, iP. SriRenganathan, Enhanced magneto-optical and photo-catalytic properties of transition metal cobalt (Co2+ions) doped spinel MgFe2O4 ferrite nanocomposites, J. Magn. Magn. Mater. 452 (2018) 380-388

[5] M.S. Hossain, B. Alam, M. Shahjahan, Synthesis , structural investigation , dielectric and magnetic properties of Zn^{2+} -doped cobalt ferrite by the sol – gel technique, 8 (2018) 2–7.

[6] A. Manikandan, S. Arul Antony, A Novel Approach for the Synthesis and Characterization Studies of Mn **2 +** -Doped CdS Nanocrystals by a Facile Microwave-Assisted Combustion Method, Journal of Superconductivity and Novel Magnetism 27 (2014) 2725-2733.

[7] D.-L. Zhao, Q. Lv, Z.M. Shen Fabrication and microwave absorbing properties of Ni–Zn spinel ferrites, J. Alloys Compd. 480 (2009) 634–638.

[8] M.K. Zate, V. V Jadhav, S.K. Gore, J.H. Shendkar, S.U. Ekar, A. Al-Osta, M. Naushad, R.S. Mane, Structural, morphological and electrochemical supercapacitive properties of sprayed manganese ferrite thin film electrode, J. Anal. Appl. Pyrolysis 122 (2016) 224–229.

[9] F. Li, J. Liu, D.G. Evans, X. Duan, Stoichiometric Synthesis of Pure MFe_2O_4 (M = Mg, Co, and Ni) Spinel Ferrites from Tailored Layered Double Hydroxide (Hydrotalcite-Like) Precursors, Chem. Mater. 16 (2004) 1597–1602.

[10] V.K. Mande, V.K. Mande, D.N. Bhoyar, S.K. Vyawahare, K. M.Jadhav, Effect of Zn^{2+} – Cr^{3+} substitution on structural, morphological, magnetic and electrical properties of $NiFe_2O_4$ ferrite nanoparticles, J. Mater. Sci. Mater. Electron. 29 (2018) 15259–15270.

[11] M. M. L. Sonia, S. Anand, V.M. Vinosel, M.A. Janifer, S. Pauline, A. Manikandan, Effect of lattice strain on structure, morphology and magneto-dielectric properties of spinel $NiGd_xFe_{2-x}O_4$ ferrite nano-crystallites synthesized by sol-gel route, J. Magn. Magn. Mater 466 (2018) 238-251.

[12] C. Srinivas, Structural and magnetic characterization of co-precipitated $Ni_xZn_{1-x}Fe_2O_4$ ferrite nanoparticles, J. Magn. Magn. Mater. 407 (2016) 135–141.

[13] C. Stergiou, Magnetic, dielectric and microwave absorption properties of rare earth doped Ni–Co and Ni–Co–Zn spinel ferrites, J. Magn. Magn. Mater. 426 (2017) 629–635.

[14] M. Ajmal, M.U. Islam, G.A. Ashraf, M.A. Nazir, M.I. Ghouri, The influence of Ga doping on structural magnetic and dielectric properties of $NiCr_{0.2}Fe_{1.8}O_4$ spinel ferrite, Physica. B. Condens. Matter. 526 (2017) 149–154.

[15] N. Lwin, M.N.A. Fauzi, S. Sreekantan, R. Othman, Physical and electromagnetic properties of nanosized Gd substituted Mg–Mn ferrites by solution combustion method, Phys. B Condens. Matter. 461 (2015) 134–139.

[16] A.A. Sattar, A.H. Wafik, K.M. El-shokrofy, Magnetic Properties of Cu ± Zn Ferrites Doped with Rare Earth Oxides, Phys. Stat. Sol. (a) 171 (1999) 563–570.

[17] K. V Zipare, S.S. Bandgar, G.S. Shahane, Effect of Dy-substitution on structural and magnetic properties of MnZn ferrite nanoparticles, J. Rare Earths. 36 (2018) 86–94.

[18] M.H. Abdellatif, M.H. Abdellatif, G.M. El-Komy, A.A. Azab, Magnetic characterization of rare earth doped spinel ferrite. J. Magn. Magn. Mater. 442 (2017) 445–452.

[19] M. Hashim, M. Raghasudha, S.S. Meena, J. Shah, S.E. Shirsath, S. Kumar, D. Ravinder, P. Bhatt, Alimuddin, R. Kumar, R.K. Kotnala, Influence of rare earth ion doping (Ce and Dy) on electrical and magnetic properties of cobalt ferrites, J. Magn. Magn. Mater. 449 (2018) 319–327.

[20] G. Dascalu, T. Popescu, M. Feder, O.F. Caltun, Structural, electric and magnetic properties of $CoFe_{1.8}RE_{0.2}O_4$ (RE=Dy, Gd, La) bulk materials, J. Magn. Magn. Mater. 333 (2013) 69–74.

[21] R.A. Pawar, S.S. Desai, S.M. Patange, S.S. Jadhav, K.M. Jadhav, Inter-atomic bonding and dielectric polarization in Gd^{3+} incorporated Co-Zn ferrite nanoparticles, Phys. B Condens. Matter. 510 (2017) 74–79.

[22] A.M. Pachpinde, M.M. Langade , K.S. Lohar, S.M. Patange, S.E. Shirsath Impact of larger rare earth Pr^{3+} ions on the physical properties of chemically derived $Pr_xCoFe_{2-x}O_4$ nanoparticles, Chem. Phys. 429 (2014) 20–26.

[23] R.K. Singh, J. Shah, R.K. Kotnala, Magnetic and dielectric properties of rare earth substituted $Ni_{0.5}Zn_{0.5}Fe_{1.95}R_{0.05}O_4$ (R = Pr, Sm and La) ferrite nanoparticles, Mater. Sci. Eng. B, Solid-State Mater. Adv. Technol. 210 (2016) 64–69.

[24] P.K. Roy, B.B. Nayak, J. Bera, J. Study on electro-magnetic properties of La substituted Ni–Cu–Zn ferrite synthesized by auto-combustion method, J. Magn. Magn. Mater. 320 (2008) 1128–1132.

[25] S. Urcia-Romero, O. Perales-Pérez, G. Gutiérrez, Effect of Dy-doping on the structural and magnetic properties of Co–Zn ferrite nanocrystals for magnetocaloric applications, J. Appl. Phys. 107 (2010) 1211–1211.

[26] A. Baykal, N. Kasapoglu, Y. Koseoglu, M.S. Toprak, H. Bayrakdar, CTAB-assisted hydrothermal synthesis of $NiFe_2O_4$ and its magnetic characterization, J. Alloys Compd. 464 (2008) 514–518.

[27] S.I. Ahmad, S.A. Ansari, D.R. Kumar, Structural, morphological, magnetic properties and cation distribution of Ce and Sm co-substituted nano crystalline cobalt ferrite, Mater. Chem. Phys. 208 (2018) 248-257.

[28] R. Waldron, Infrared spectra of ferrites, Phys. Rev. 99 (1955) 1727–1735.

[29] P. Pulišová, J. Kováč, A. Voigt, P. Raschman, Structure and magnetic properties of Co and Ni nano-ferrites prepared by a two step direct microemulsions synthesis, J. Magn. Magn. Mater. 341 (2013) 93–99.

[30] Y. Slimani, H. Güngüneş, M. Nawaz, A. Manikandan, H.S. El Sayed, M.A. Almessiere, H. Sözeri, S.E.Shirsath, I. Ercan, A. Baykal, Magneto-optical and microstructural properties of spinel cubic copper ferrites with Li-Al co substitution. Ceramics International 44 (2018) 14242–14250.

[31] E.C. Stoner, E.P. Wohlfarth, A Mechanism of Magnetic Hysteresis in Heteregeneous Alloys, Philosophical Transactions of the Royal Society A 240 (826) (1948) 599-642.

[32] M.A. Almessiere, Y. Slimani, A.Baykal, Exchange spring magnetic behavior of $Sr_{0.3}Ba_{0.4}Pb_{0.3}Fe_{12}O_{19}/(CuFe_2O_4)_x$ nanocomposites fabricated by a one-pot citrate sol-gel combustion method, Journal of Alloys and Compounds 762 (2018) 389-397.

[33] G.V. Duong, N. Hanh, D.V. Linh, R. Groessinger, P. Weinberger, E. Schafler, M. Zehetbauer, Monodispersed nanocrystalline $Co_{1-x}Zn_xFe_2O_4$ particles by forced hydrolysis: Synthesis and characterization, J. Magn. Magn. Mater. 311 (2007) 46–50.

[34] F. Gözüak, Y. Köseoglu, A. Baykal, H. Kavas, Synthesis and characterization of $Co_xZn_{1-x}Fe_2O_4$ magnetic nanoparticles via a PEG-assisted route, J. Magn. Magn. Mater. 321 (2009) 2170–2177.

[35] S.N. Rafeeq, M.M. Ismail, J.M.A. Sulaiman, Magnetic and Dielectric Properties of $CoFe_2O_4$ and $Co_xZn_{1-x}Fe_2O_4$ Nanoparticles Synthesized Using Sol-Gel Method, J. Magnetics 22 (2017) 406-413.

[36] Sanjeev Kumar, Vaishali Singh, Uttam K. Mandal, R.K. Kotnala, Nanocrystalline $Co_{0.5}Zn_{0.5}Fe_2O_4$ ferrite: Synthesis, characterization and study of their magnetic behavior at different temperatures, Inorganica Chimica Acta 428 (2015) 21-26.

[37] M.M. Rashad, R.M. Mohamed, H. El-Shall, Magnetic properties of nanocrystalline Sm-substituted $CoFe_2O_4$ synthesized by citrate precursor method, Journal of Materials Processing Technology 198 (2008) 139-146.

[38] J.M.D. Coey, Noncollinear spin arrangement in ultrafine ferrimagnetic crystallites, Phys. Rev. Lett. 27 (1971) 1140-1142.

[39] Md Amir, H. Gungunes, Y. Slimani, N. Tashkandi, H.S. El Sayed, F. Aldakheel, M. Sertkol, H. Sozeri, A. Manikandan, I. Ercan, A. Baykal, Mossbauer studies and magnetic properties of cubic $CuFe_2O_4$ nanoparticles, J. Supercond. Nov. Magn. (2018), https://doi.org/10.1007/s10948-018-4733-5.

[40] M. A. Almessiere, Y. Slimani, A. Baykal, Structural and magnetic properties of Ce doped strontium hexaferrite, Ceram Int. 44 (2018) 9000.

[41] M. A. Almessiere, Y. Slimani, H.S. El Sayed, A. Baykal, Structural and magnetic properties of Ce-Y substituted strontium nanohexaferrites. Ceram Int. 44 (2018) 12511.

[42] Y. Slimani, H. Güngüneş, M. Nawaz, A. Manikandan, H.S. El Sayed, M.A. Almessiere, H. Sözeri, S.E. Shirsath, I. Ercan, A. Baykal, Magneto-optical and microstructural properties of spinel cubic copper ferrites with Li-Al co-substitution. Ceram Int. 44 (2018) 14242.

[43] Y. Slimani, A. Baykal, Md. Amir, H. Güngüneş, S. Guner, H. S. El Sayed, F. Aldakheel, T. A. Saleh, A. Manikandan, Substitution effect of Cr^{3+} on hyperfine interactions, magnetic and optical properties of Sr-hexaferrites. Ceram Int. 44 (2018) 15995.

[44] K.K. Bamzai, G. Kour, B. Kaur, S.D. Kulkarni, Effect of cation distribution on structural and magnetic properties of Dy substituted magnesium ferrite, J. Magn. Magn. Mater. 327 (2013) 159–166.

[45] L. Zhao, H. Yang, L. Yu, Y. Cui, X. Zhao, S. Feng, Magnetic properties of Re-substituted Ni–Mn ferrite nanocrystallites, J. Mater. Sci. 42 (2007) 686–691.

[46] M.A. Almessiere, Y. Slimani, N.A. Tashkandi, A. Baykal, M.F. Saraç, A.V. Trukhanov, İ. Ercan, İ. Belenli, B. Ozçelik, The effect of Nb substitution on magnetic properties of

$BaFe_{12}O_{19}$ nanohexaferrites, Ceram. Int. (2018), https://doi.org/10.1016/j.ceramint.2018.10.048.

[47] **E.** Hema, A. Manikandan, P. Karthika, M. Durka, S.A. Antony, B.R. Venkatraman, Magneto-Optical Properties of Reusable Spinel $Ni_x Mg_{1-x}Fe_2O_4(0.0 \leq x \leq 1.0)$ Nano-Catalysts, Journal of Nanoscience and Nanotechnology 16 (2016) 7325-7336

[48] M. A. Almessiere, Y. Slimani, H. Güngüneş, H. S. El Sayed, A. Baykal, AC Susceptibility and Hyperfine Interactions of Vanadium Substituted Barium Nanohexaferrites, Ceram. Int. 44 (2018) 17749-17758.

[49] M. A. Almessiere, Y. Slimani, H. S. El Sayed, A. Baykal, I. Ercan, Microstructural and magnetic investigation of vanadium-substituted Sr-nanohexaferrite, J. Magn. Magn. Mater. 471 (2019) 124-132.

[50] Md Amir, H. Gungunes, Y. Slimani, N. Tashkandi, H.S. El Sayed, F. Aldakheel, M. Sertkol, H. Sozeri, A. Manikandan, I. Ercan, A. Baykal, Mossbauer studies and magnetic properties of cubic $CuFe_2O_4$ nanoparticles, J. Supercond. Nov. Magn. (2018), https://doi.org/10.1007/s10948-018-4733-5.

[51] A.D. Korkmaz, S. Güner, Y. Slimani, H. Gungunes, Md. Amir, A. Manikandan, A. Baykal, Microstructural, optical and magnetic properties of vanadium substituted nickel spinel nano-ferrites, J. Supercond. Nov. Magn. (2018), https://doi.org/10.1007/s10948-018-4793-6.

[52] M.A. Almessiere, Y. Slimani, A. Baykal, Exchange spring magnetic behavior of $Sr_{0.3}Ba_{0.4}Pb_{0.3}Fe_{12}O_{19}/(CuFe_2O_4)_x$ nanocomposites fabricated by a one-pot citrate sol-gel combustion method, J. Alloys Compd. 762 (2018) 389–39.

List of Figures

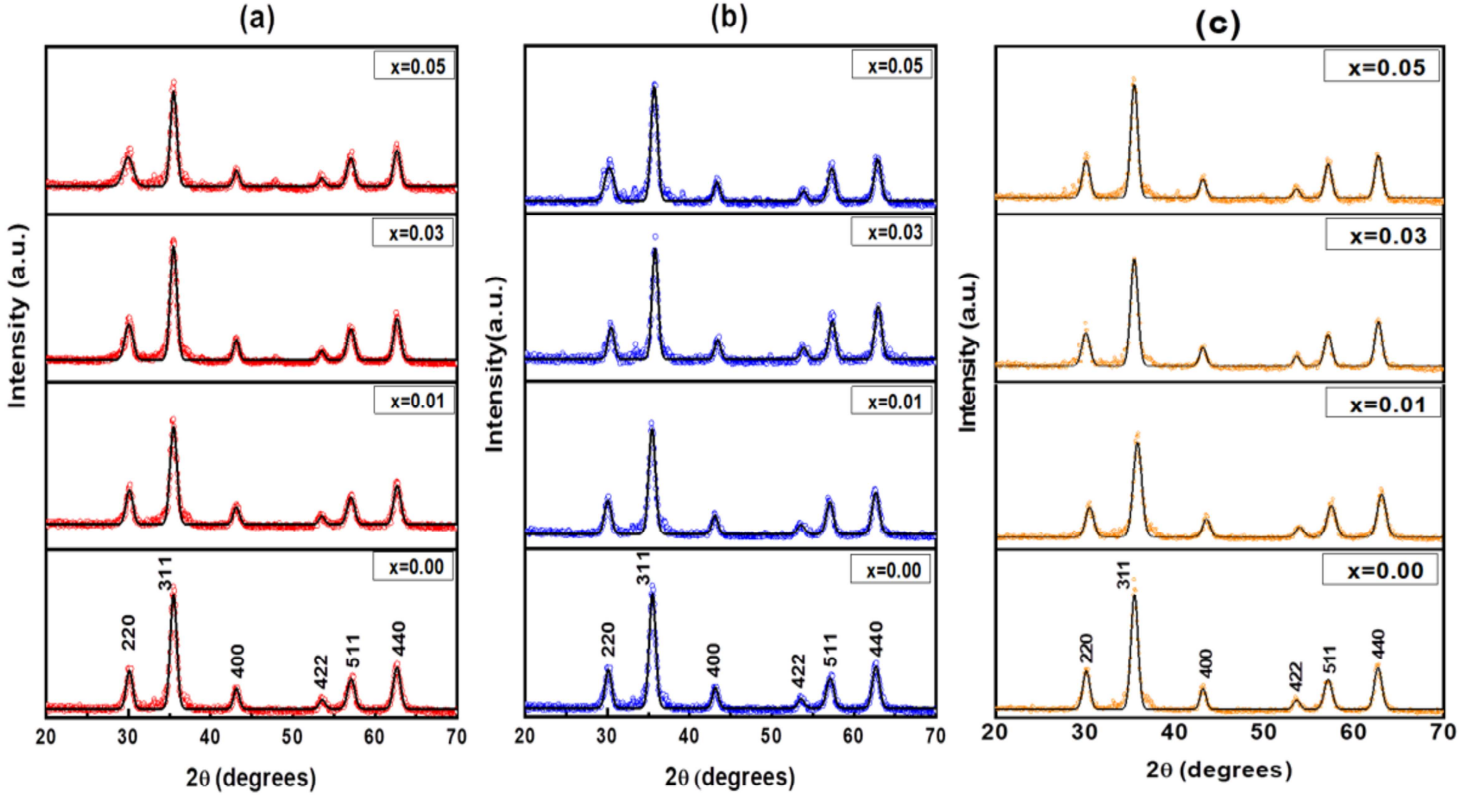
(a)
(b)
(c)
x=0.05
x=0.03
x=0.01
x=0.00
Intensity (a.u.)
Intensity(a.u.)
220
311
400
422
511
440
20
30
40
50
60
70
2θ (degrees)

Fig. 1.

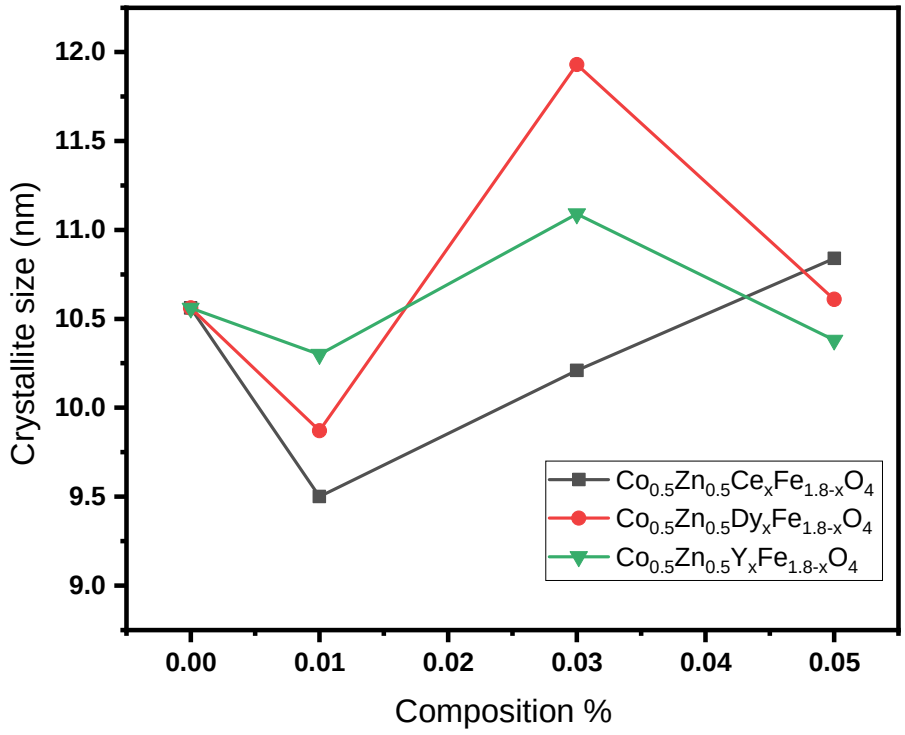
12.0
11.5
11.0
10.5
10.0
9.5
9.0
Crystallite size (nm)
0.00
0.01
0.02
0.03
0.04
0.05
Composition %
Co0.5Zn0.5CexFe1.8-xO4
Co0.5Zn0.5DyxFe1.8-xO4
Co0.5Zn0.5YxFe1.8-xO4

Fig. 2.

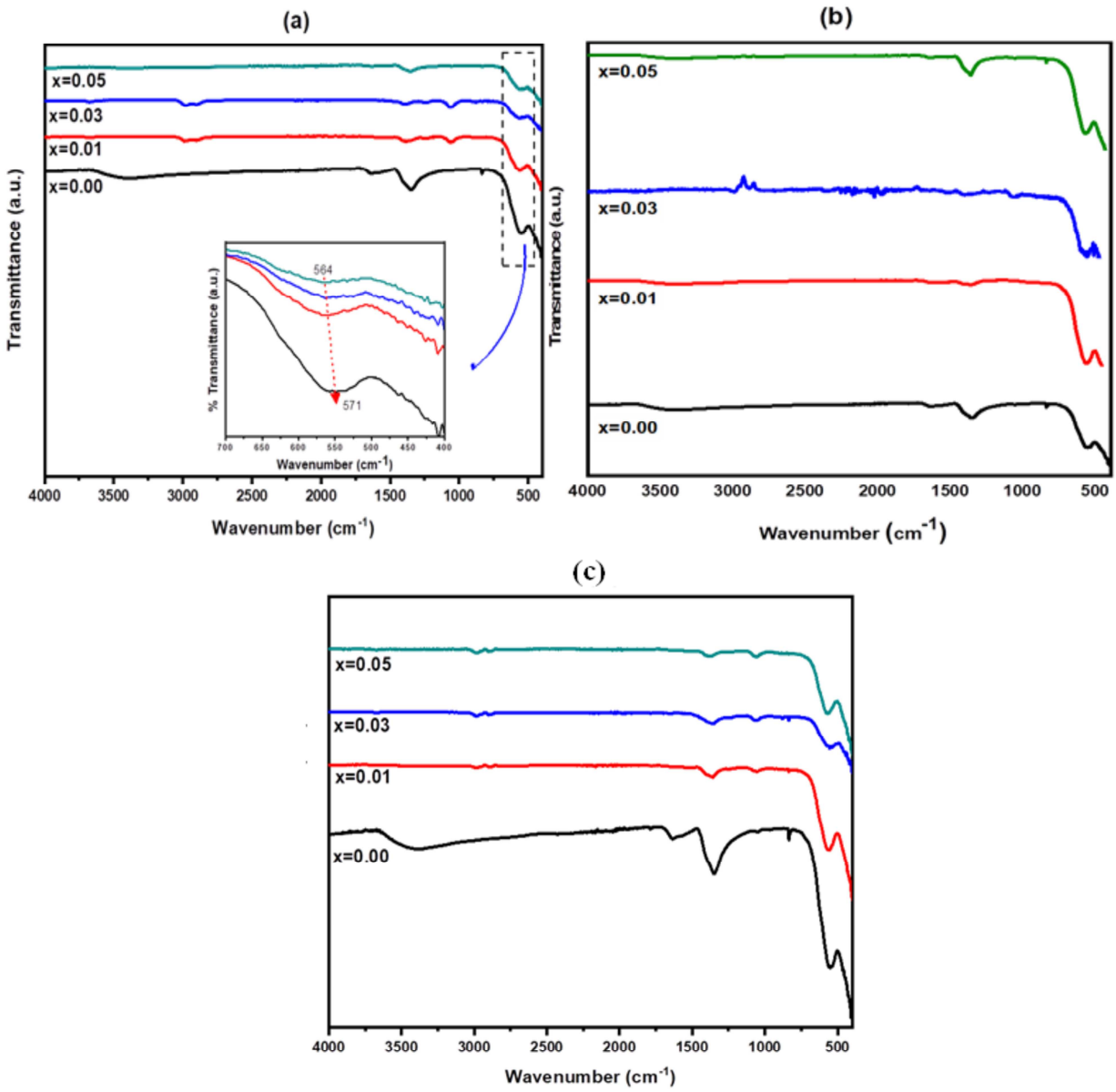
(a)
x=0.05
x=0.03
x=0.01
x=0.00
Transmittance (a.u.)
Wavenumber (cm-1)
564
571
% Transmittance (a.u.)
(b)
x=0.05
x=0.03
x=0.01
x=0.00
Transmittance (a.u.)
Wavenumber (cm-1)
(c)
x=0.05
x=0.03
x=0.01
x=0.00
Wavenumber (cm-1)

Fig. 3.

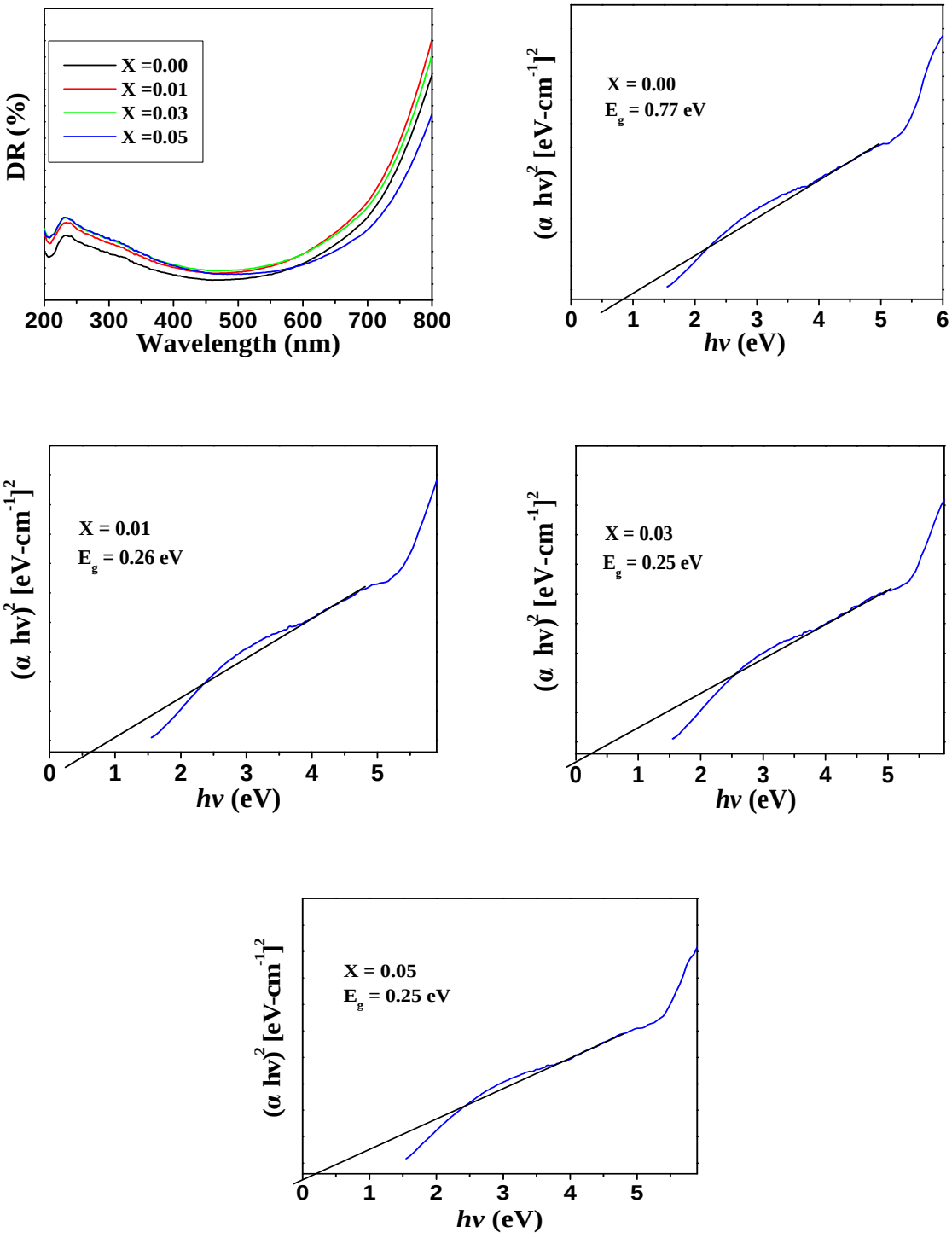
X =0.00
X =0.01
X =0.03
X =0.05
DR (%)
Wavelength (nm)
200 300 400 500 600 700 800
X = 0.00
E_g = 0.77 eV
(α hν)^2 [eV-cm^-1]^2
hν (eV)
0 1 2 3 4 5 6
X = 0.01
E_g = 0.26 eV
X = 0.03
E_g = 0.25 eV
X = 0.05
E_g = 0.25 eV
0 1 2 3 4 5

Fig. 4.

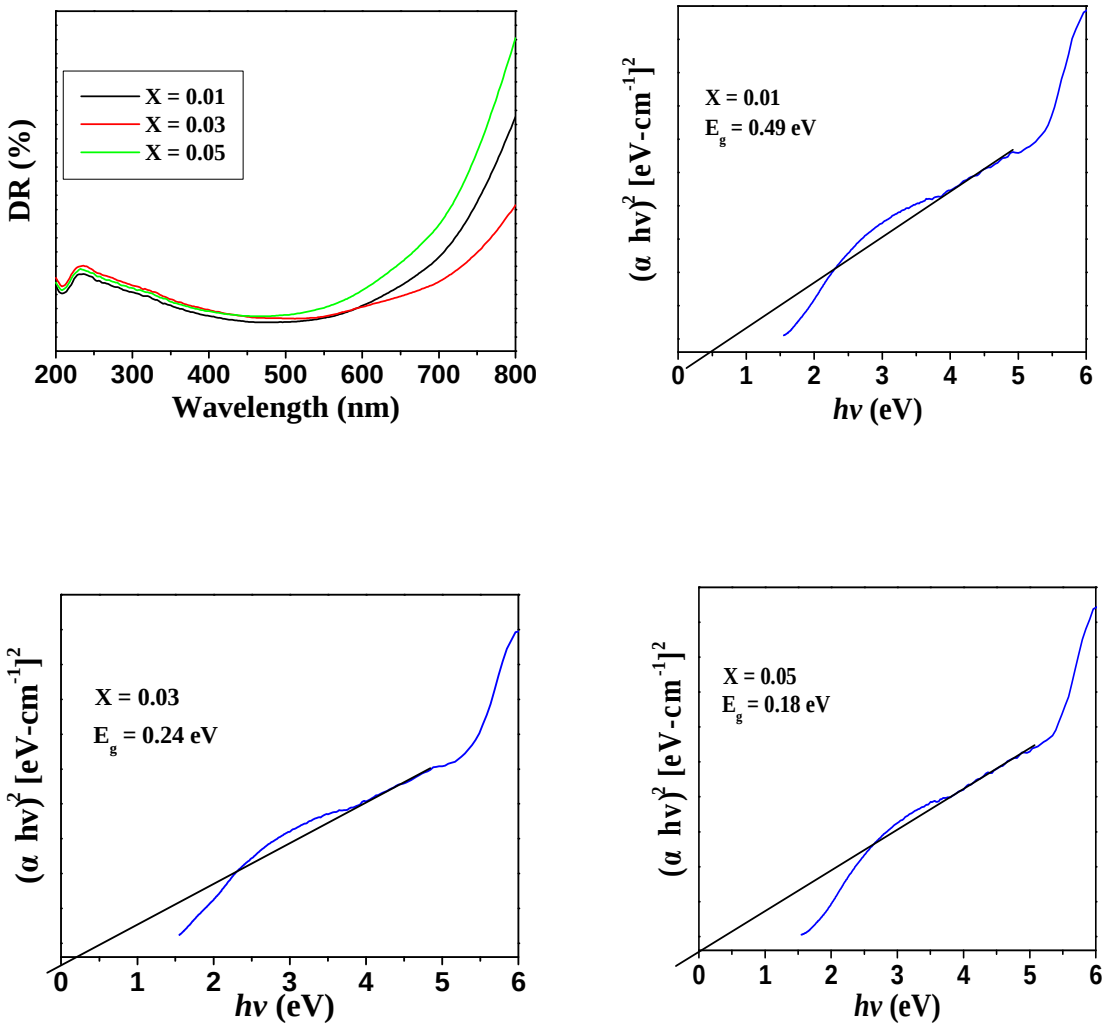
X = 0.01
X = 0.03
X = 0.05
DR (%)
Wavelength (nm)
200 300 400 500 600 700 800
X = 0.01
E_g = 0.49 eV
(α hν)^2 [eV-cm^-1]^2
hν (eV)
0 1 2 3 4 5 6
X = 0.03
E_g = 0.24 eV
X = 0.05
E_g = 0.18 eV

Fig. 5.

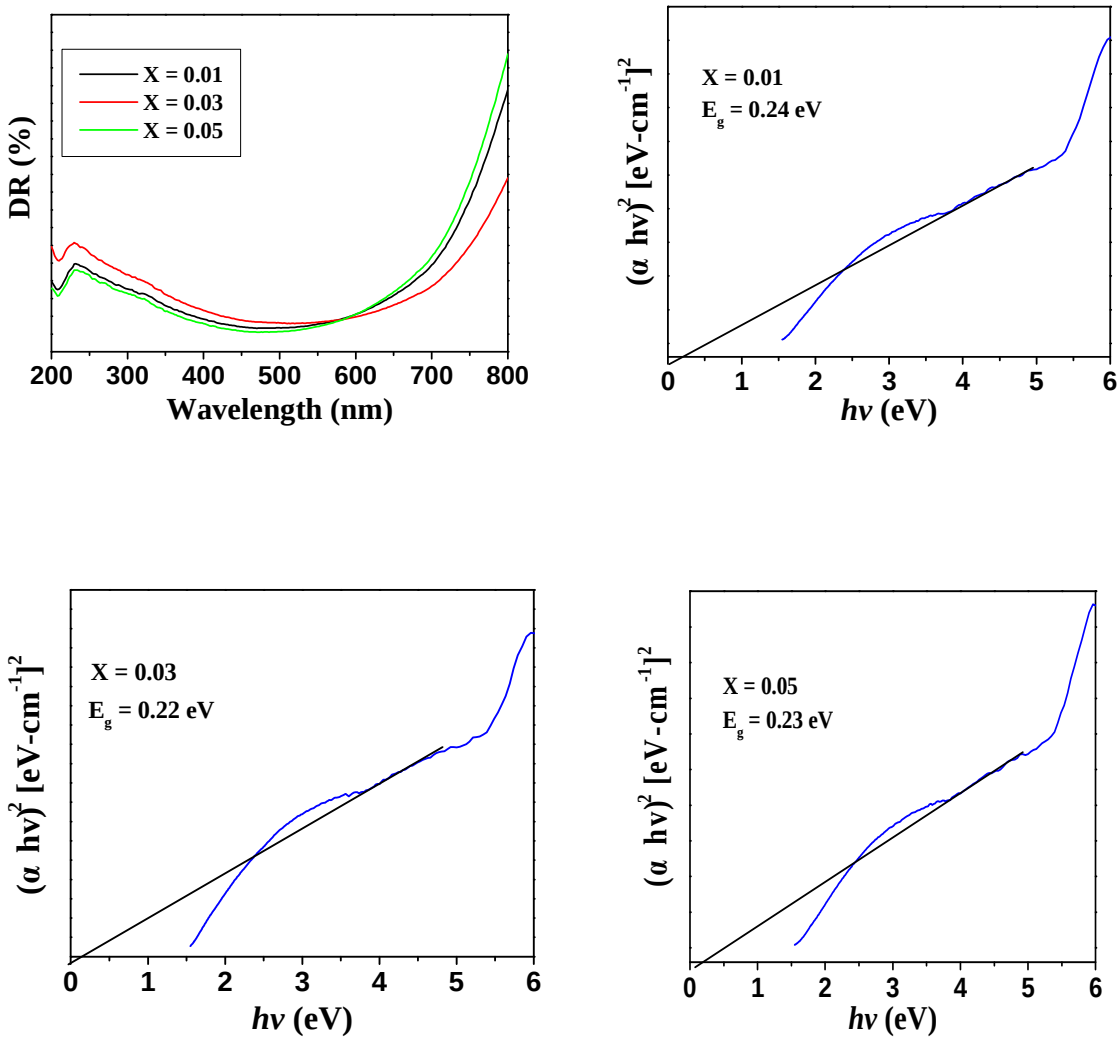
X = 0.01
X = 0.03
X = 0.05
DR (%)
Wavelength (nm)
200 300 400 500 600 700 800
X = 0.01
E_g = 0.24 eV
(α hν)^2 [eV-cm^-1]^2
hν (eV)
0 1 2 3 4 5 6
X = 0.03
E_g = 0.22 eV
X = 0.05
E_g = 0.23 eV

Fig. 6.

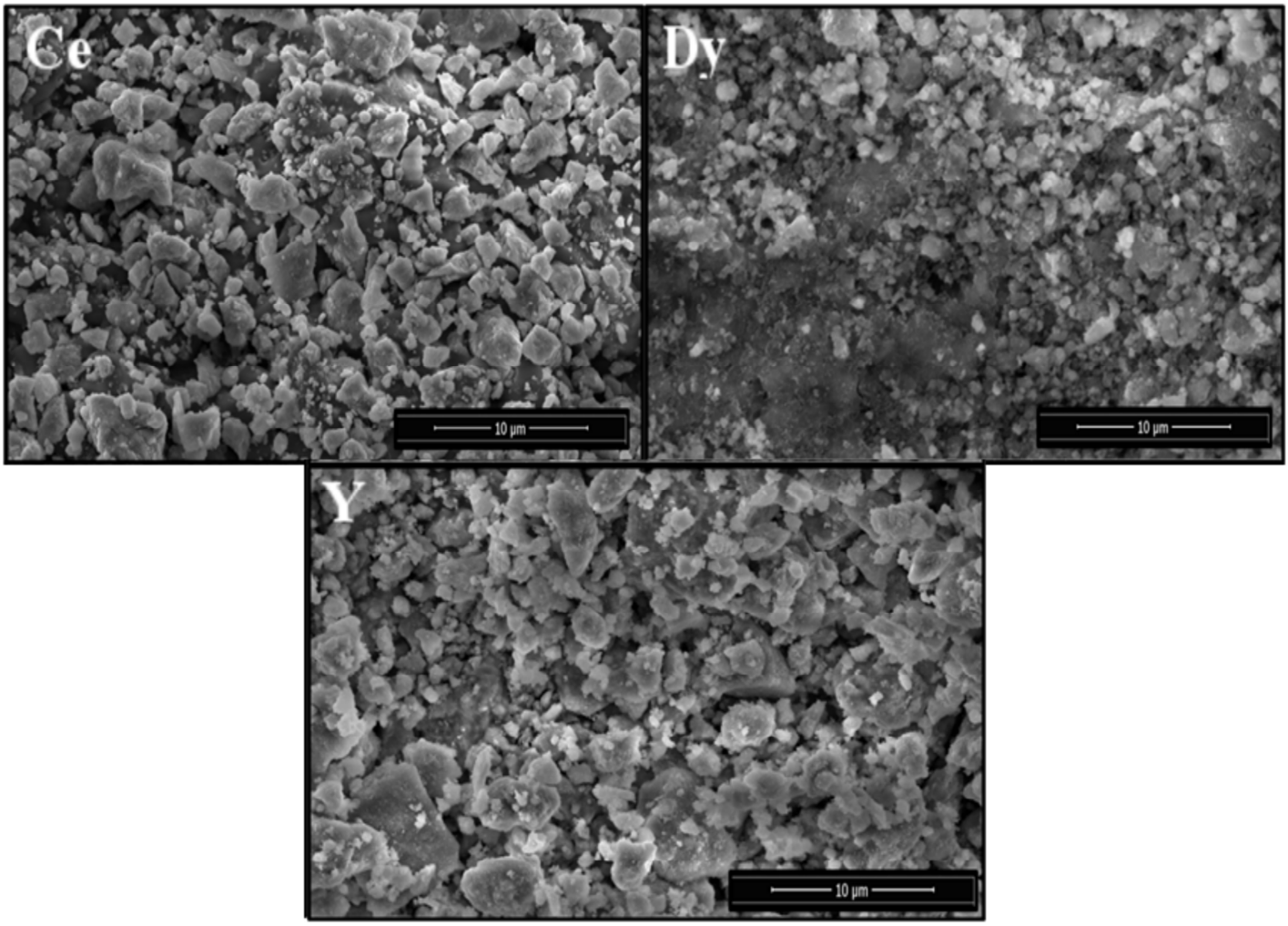

Fig. 7.

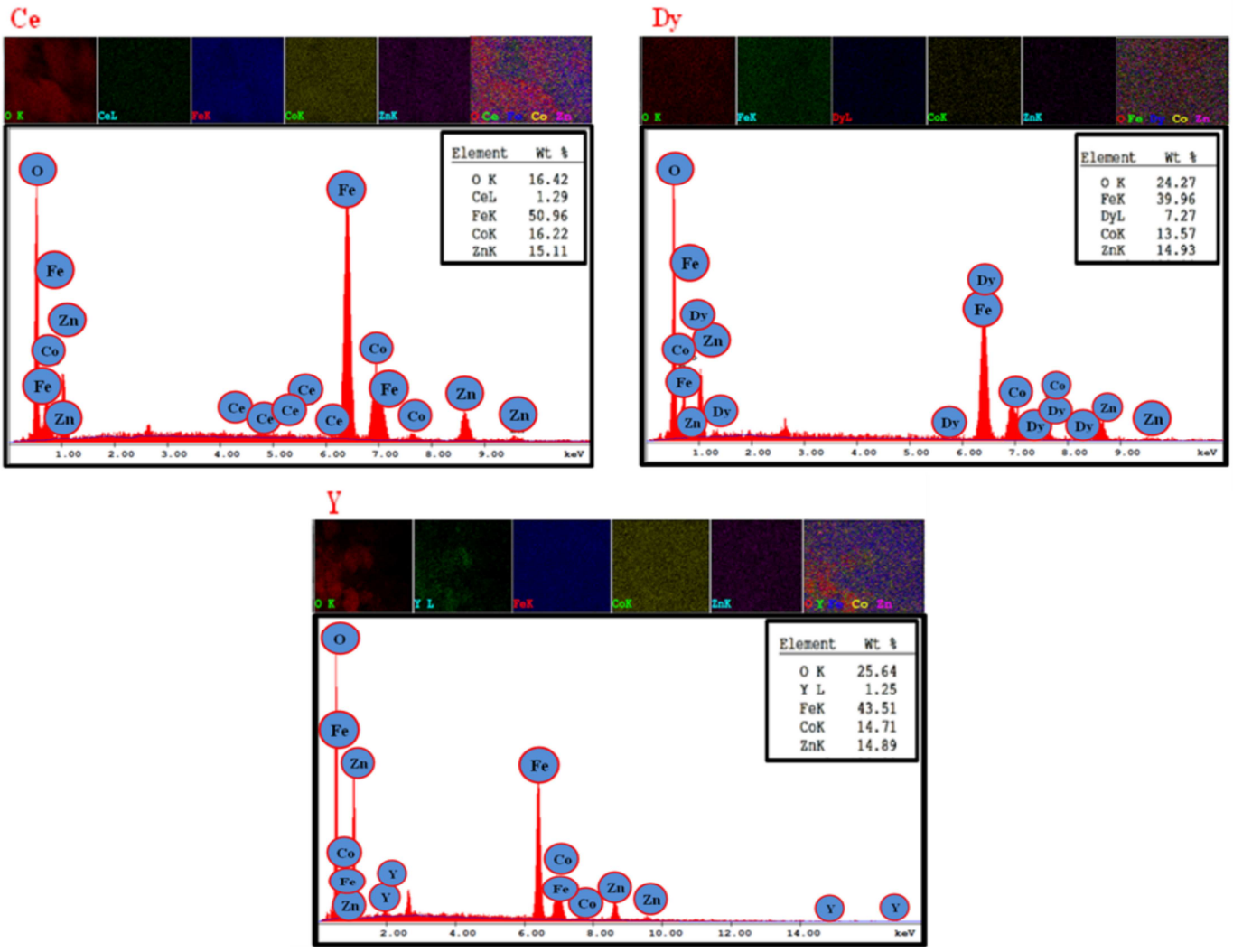
Ce
O K
CeL
FeK
CoK
ZnK
O Ce Fe Co Zn
Element Wt %
O K 16.42
CeL 1.29
FeK 50.96
CoK 16.22
ZnK 15.11
O
Fe
Zn
Co
Ce
1.00 2.00 3.00 4.00 5.00 6.00 7.00 8.00 9.00 keV
Dy
O K
FeK
DyL
CoK
ZnK
O Fe Dy Co Zn
Element Wt %
O K 24.27
FeK 39.96
DyL 7.27
CoK 13.57
ZnK 14.93
O
Fe
Dy
Zn
Co
1.00 2.00 3.00 4.00 5.00 6.00 7.00 8.00 9.00 keV
Y
O K
Y L
FeK
CoK
ZnK
O Fe Co Zn
Element Wt %
O K 25.64
Y L 1.25
FeK 43.51
CoK 14.71
ZnK 14.89
O
Fe
Zn
Co
Y
2.00 4.00 6.00 8.00 10.00 12.00 14.00 keV

Fig. 8.

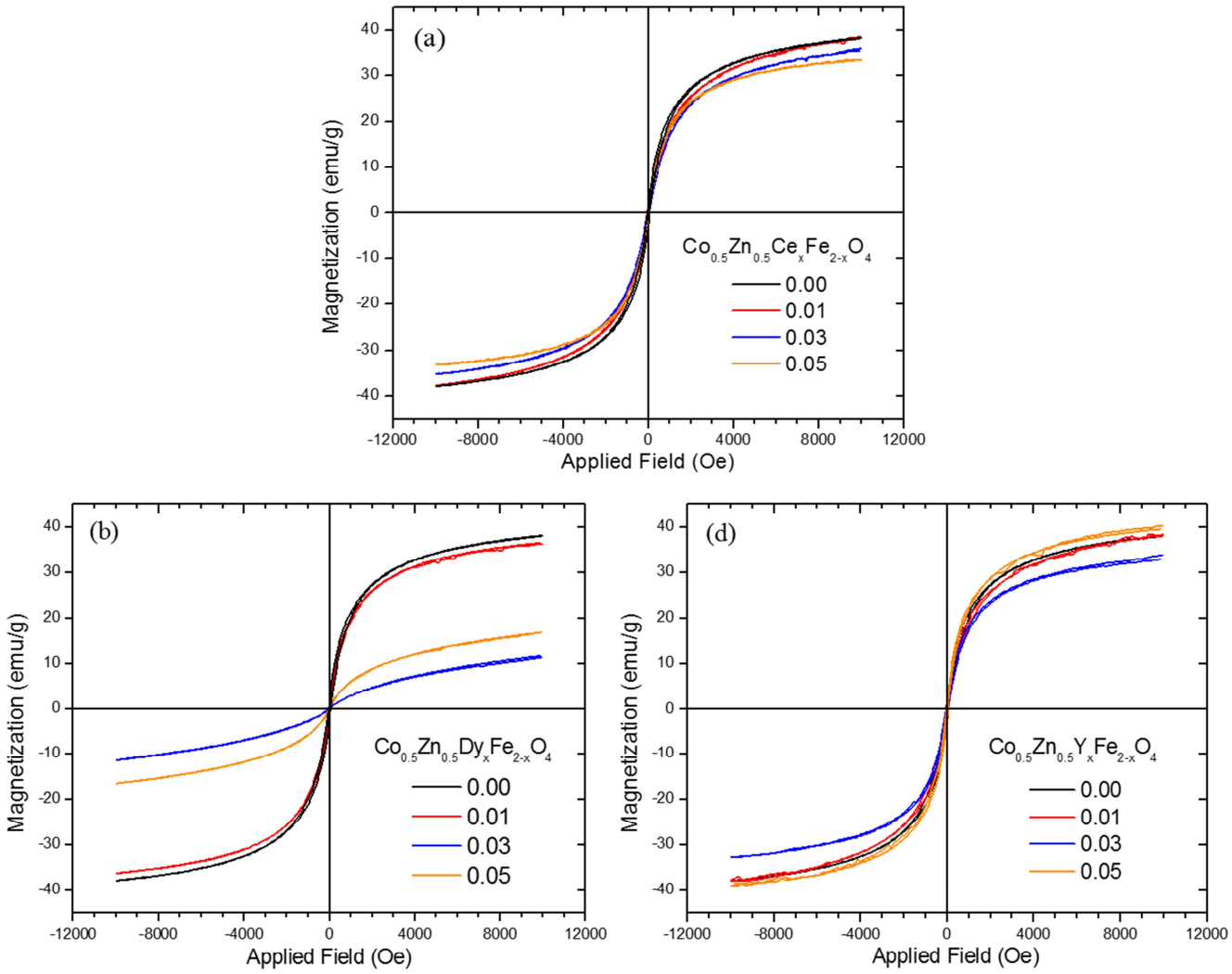
(a)
Magnetization (emu/g)
Applied Field (Oe)
Co0.5Zn0.5CexFe2-xO4
0.00
0.01
0.03
0.05
(b)
Magnetization (emu/g)
Applied Field (Oe)
Co0.5Zn0.5DyxFe2-xO4
0.00
0.01
0.03
0.05
(d)
Magnetization (emu/g)
Applied Field (Oe)
Co0.5Zn0.5YxFe2-xO4
0.00
0.01
0.03
0.05

Fig. 9.

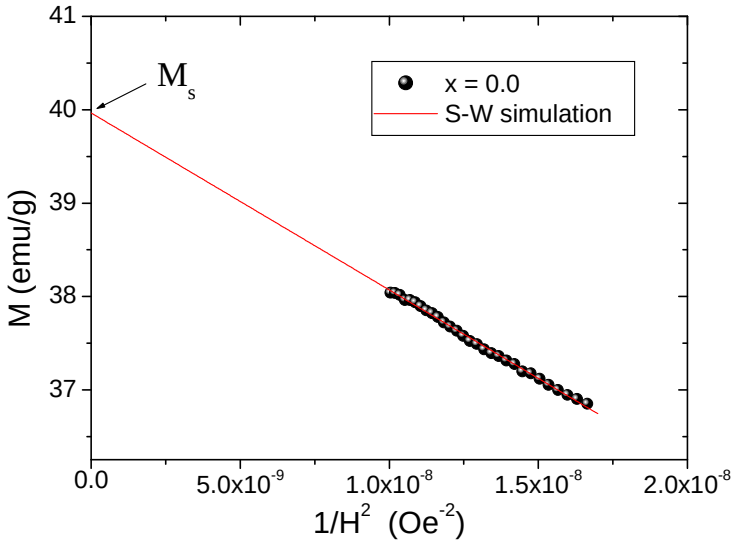
41
40
39
38
37
M (emu/g)
M$_s$
x = 0.0
S-W simulation
0.0
5.0x10^{-9}
1.0x10^{-8}
1.5x10^{-8}
2.0x10^{-8}
1/H^2 (Oe^{-2})

Fig. 10.

List of Tables

Table Captions

Table 1.

	a (Å)				D_{XRD} (nm)			
Samples	**0.00**	**0.01**	**0.03**	**0.05**	**0.00**	**0.01**	**0.03**	**0.05**
$Co_{0.5}Zn_{0.5}Ce_xFe_{2-x}O_4$	8.400	8.3904	8.3753	8.3792	10.6	11.3	10.1	9.4
$Co_{0.5}Zn_{0.5}Dy_xFe_{2-x}O_4$	8.400	8.3753	8.3871	8.3727	10.6	9.9	7.5	8.5
$Co_{0.5}Zn_{0.5}Y_xFe_{2-x}O_4$	8.400	8.3781	8.3974	8.3902	10.6	11.2	9.0	11.7

Table 2.

	M_s (emu·g^{-1})			M_r (emu·g^{-1})			SQR			H_c (Oe)			n_B (μ_B)		
RE / x	Ce	Dy	Y	Ce	Dy	Y	Ce	Dy	Y	Ce	Dy	Y	Ce	Dy	Y
0.00	39.9	39.9	39.9	2.03	2.03	2.03	0.051	0.051	0.051	50.5	50.5	50.5	1.70	1.70	1.70
0.01	40.8	37.8	40.2	2.20	1.17	2.18	0.054	0.031	0.054	43.1	29.2	47.2	1.74	1.61	1.72
0.03	37.5	13.6	35.2	1.70	0.16	1.64	0.045	0.012	0.047	53.8	37.3	61.2	1.61	0.58	1.50
0.05	34.7	18.7	41.8	0.23	0.30	2.51	0.007	0.016	0.060	57.3	25.2	31.9	1.50	0.81	1.80